Journal of Mechanics in Medicine and Biology
Vol. 19, No. 1 (2019) 1950014 (13 pages)

DOI: 10.1142/S0219519419500143

COMPUTATIONAL STUDY ON THE RUPTURE RISK IN REAL CEREBRAL ANEURYSMS WITH GEOMETRICAL AND FLUID-MECHANICAL PARAMETERS USING FSI SIMULATIONS AND MACHINE LEARNING ALGORITHMS

ALFREDO ARANDA* and ALVARO VALENCIA

Department of Mechanical Engineering
Universidad de Chile, Beauchef 851
Santiago 8370456, Chile
**alfredo.arandan@gmail.com*

Received 27 May 2018
Revised 15 October 2018
Accepted 26 October 2018
Published 27 February 2019

Fluid-mechanical and morphological parameters are recognized as major factors in the rupture risk of human aneurysms. On the other hand, it is well known that a lot of machine learning tools are available to study a variety of problems in many fields. In this work, fluid–structure interaction (FSI) simulations were carried out to examine a database of 60 real saccular cerebral aneurysms (30 ruptured and 30 unruptured) using reconstructions by angiography images. With the results of the simulations and geometric analyses, we studied the analysis of variance (ANOVA) statistic test in many variables and we obtained that aspect ratio (AR), bottleneck factor (BNF), maximum height of the aneurysms (MH), relative residence time (RRT), Womersley number (WN) and Von-Mises strain (VMS) are statically significant and good predictors for the models. In consequence, these ones were used in five machine learning algorithms to determine the rupture risk predictions of the aneurysms, where the adaptative boosting (AdaBoost) was calculated with the highest area under the curve (AUC) in the receiver operating characteristic (ROC) curve (AUC 0.944).

Keywords: Machine learning; FSI simulations; cerebral aneurysm simulations; statistic predictions; statistical significance; computational applications.

1. Introduction

An intracranial cerebral aneurysm is an abnormal dilation of an artery caused by a weakness in their located in the subarachnoid space at the base.[1,2] These are typically classified based on its form and position in the main artery into terminal, lateral (saccular), or bifurcation aneurysm.[3] Many factors, such as high-blood

*Corresponding author.

pressure, smoking, family history and stress out may influence or increase the risk of rupture.[2] The cerebral aneurysm may be deadly whether this one has a rupture, for this reason, it is essential and may be able to predict the rupture risk. Clinical studies regarding the behavior of hemodynamic parameters such as the wall shear stress (WSS), the geometric parameters or the interior velocity field within the aneurysm may be occasionally difficult to measure, having an important role in the rupture.[4–7] In contrast, a complete aneurysm statistic and fluid-dynamic studies (some results may be read in Refs. 8–10) are possible via computational fluid dynamic (CFD) and fluid–structure interaction simulations (FSI) reconstructing cerebral aneurysm of patients,[11] allowing to predict the rupture risk with machine learning tools. Shum *et al.*[12] found in an assessment of AAA rupture risk using machine learning that the null hypothesis is rejected when geometrical factors are considered predictors in a classify model. Muluk *et al.*[13] predicted the aortic aneurysm rupture using only geometric parameters considering 15 variables. In the same way, Mocco *et al.*[7] used the aneurysm morphology to demonstrate and predict that these ones can be good predictors. In addition, a recent study of Liu *et al.*[14] predicted the rupture risk using morphological parameters and healthy behaviors. In this investigation, we carried out five supervised machine learning algorithms using fluid-mechanical and morphological variables to predict the rupture risk of the cerebral aneurysm, choosing the best one of them.

2. Methods

2.1. *Reconstruction of geometries and morphological parameters*

According to the simulations, we reconstructed real aneurysms using angiography images located in different cerebral regions: the pericallosal artery, the middle cerebral artery, the internal carotid artery, the basilar artery, the posterior communicating artery and the posterior inferior cerebellar artery.

The computational geometries of arteries were generated by first performing aneurysm surgeries of the patients of Instituto de Neurocirugía Asenjo (INCA), and then reconstructing 60 three-dimensional angiography images on a 1:1 scale, following the procedure described by Valencia *et al.*[15] A result is shown in Fig. 1. In this investigation, 30 aneurysms ruptured and 30 unruptured were reconstructed and used in the simulations on the Ansys software.

Geometrical parameters of all aneurysms are shown in Fig. 1(b) with their respective statistics in Table 1 (in mm). We also calculated four morphological parameters to characterize the aneurysm: The aspect ratio (AR) the bottleneck factor (BNF), the nonsphericity index (NSI) and the aneurysm inclination angle (AIA) (for more details see Ref. 16), where the statistic values are shown in Table 1, in addition, we presented some general characteristics such as age, surface area of the aneurysm (SAA in mm^2) and volume of the aneurysm (VA in mm^3).

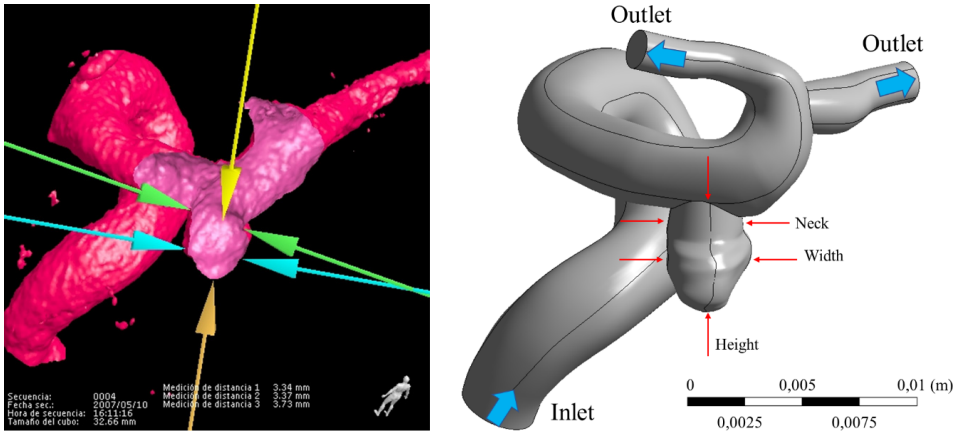

Fig. 1. (a) Three-dimensional angiography image from a patient of INCA, (b) reconstruction from the three-dimensional angiography with inlet and outlets and the aneurysm geometrical measurement (neck, width, height and the aneurysm inclination angle).

Table 1. Statistical values for the geometrical parameters.

Statistic	Neck	Width	Height	AR	BNF	NSI	AIA	Age	SSA	VA
Min.	1.08	1.17	1.48	0.6337	0.5745	0.1157	0.0008	29	5.72	2.84
Max.	9.72	12.7	11.37	5.2786	6.3159	0.5119	0.1963	81	341.94	542.51
Median	3.59	5.16	5.78	1.5055	1.3307	0.2967	0.1130	57	105.33	81.34
Mean	3.72	5.45	5.60	1.6595	1.5954	0.2957	0.1051	58	107.36	103.77
St. Dev.	1.61	2.68	2.35	0.8328	0.8995	0.0513	0.0544	11	79.64	105.65

According to the AIA, we defined the maximum high (MH) of the aneurysm as $\mathrm{MH} = \frac{\mathrm{Height}}{\mathrm{AIA}}$.

2.2. *Computational and numerical methods*

The blood inside the small brain arteries was considered as a laminar, incompressible and non-Newtonian fluid, using $\rho = 1065\,\mathrm{kg/m^3}$ (Refs. 17 and 18) and the Carreau rheological model (shown in Eq. (1)) to obtain the shear thinning behavior.[19,20]

$$\mu_{\mathrm{eff}}(\dot{\gamma}) = \mu_{\mathrm{inf}} + (\mu_0 - \mu_{\mathrm{inf}})(1 + (\lambda\dot{\gamma})^2)^{\frac{n-1}{2}}, \tag{1}$$

where $\mu_{\mathrm{inf}} = 0.00345\,\mathrm{kg/m{\cdot}s}$ (viscosity at infinite shear rate), $\mu_0 = 0.056\,\mathrm{kg/m{\cdot}s}$ (viscosity at zero shear rate), $\lambda = 3.313s$ (relaxation time), and $n = 0.3568$ (power index) are the material coefficients.

For the artery wall, we considered a density $\rho = 1050\,\mathrm{kg/m^3}$ (Refs. 21–23) and an hyperelastic material, considering the Mooney–Rivlin five parameters models

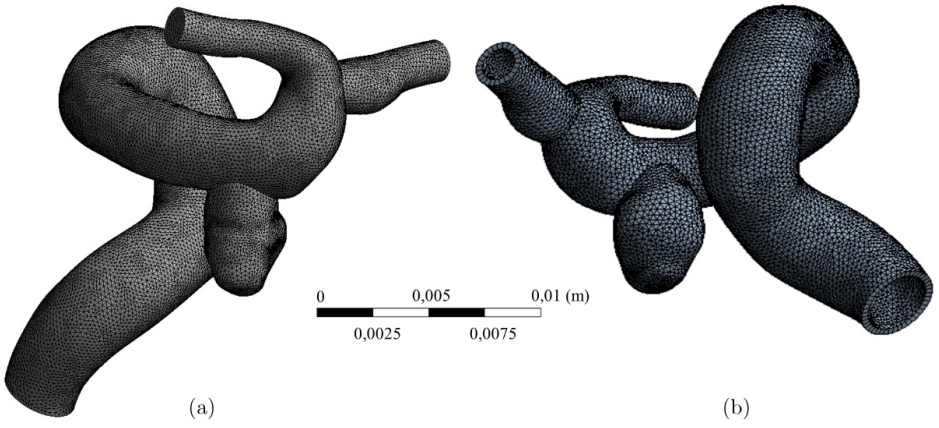

Fig. 2. (a) Tetrahedral mesh for the Ansys Fluent using 1500 elements/mm^3. (b) Triangle mesh for the Ansys Transient Structural using 100 elements/mm^2. Both results were considered in all geometries.

(shown in Eq. (2)), where we followed the results measured by Valencia *et al.*[24] For the thickness of each aneurysm we considered 0.35 mm.[25]

$$w = C_{10}(\bar{I}_1 - 3) + C_{01}(\bar{I}_2 - 3) + C_{11}(\bar{I}_1 - 3)(\bar{I}_2 - 3) + C_{20}(\bar{I}_1 - 3)^2 + C_{02}(\bar{I}_2 - 3)^2, \quad (2)$$

where $\bar{I}_1$, $\bar{I}_2$ are the strain invariants, $C_{10} = 0.4286$ MPa, $C_{01} = -0.1185$ MPa, $C_{11} = 0.5847$ MPa, $C_{20} = 0.5793$ MPa, $C_{02} = 0.5638$ MPa.[24]

We configured a tetrahedral mesh for fluid simulations and triangles mesh for structural simulations (shown in Figs. 2(a) and 2(b)) solving the transient Navier–Stokes equations coupled with the transient mechanical equations. We also used a mesh density of 1500 elements/mm^3 for fluid in accordance with the study of the WSS at the systole time with 250, 500, 1000, 2500, 3500 and 4500 elements/mm^3, respectively. The maximum difference is shown Fig. 3, being below 2% between 1500 and 4500 elements/mm^3. The similar study was realized with Ansys Transient Structural simulations considering the equivalent strain (Von-Mises) at the systole, resulting an optimal value of 100 elements/mm^2 (Fig. 3(b)).

The criteria values selected for the time step and residual were 0.0001 s and 0.001 for the FSI simulations, respectively.

The solutions of two-way surface force/displacement coupling with Ansys Fluent and Ansys Mechanical were implemented in the FSI simulations,[26] using a dynamic mesh with a smoothing method (diffusion parameter equal to 2). For the structure deformation, we used a FEM. On the other hand, the pressure implicit with splitting of operator (PISO) algorithm was used to solve the Navier–Stokes equations using the spatial discretization of the least squares cell based on the gradient, second-order pressure, and second-order upwind for the momentum. For the transient formulation, the second-order implicit method was used.

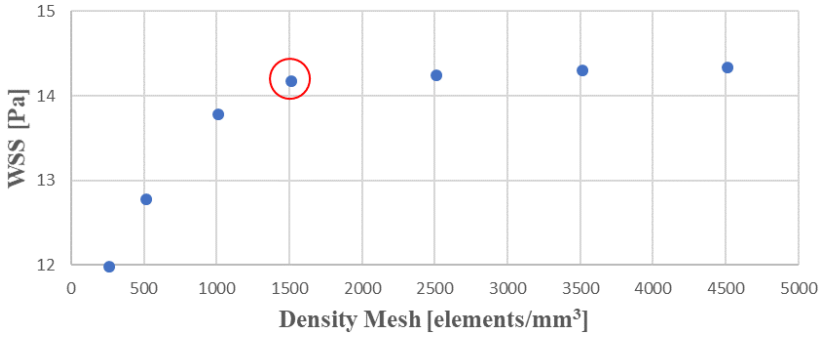

Fig. 3. Comparison of mesh results when WSS at systole time was calculated using different mesh densities. The difference of the computing time in ANSYS was almost 10 times between 4500 and 1500 elements/mm^3.

We also calculated the relative residence time (RRT) (Eq. (3)) to relate the time-averaged wall shear stress (TAWSS) and the oscillatory shear index (OSI),[27,28] where each quantity was besides averaged over the area of each aneurysm during a cardiac cycle T.

$$\mathrm{RRT} = \frac{1}{(1 - 2 \times \mathrm{OSI}) \times \mathrm{TAWSS}} \tag{3}$$

where $\mathrm{OSI} = \frac{1}{2}\left(1 - \frac{\left|\int_0^T \tau_w(\mathbf{x},t)dt\right|}{\int_0^T |\tau_w(\mathbf{x},t)|dt}\right)$ and $\mathrm{TAWSS} = \frac{1}{T}\int_0^T |\tau_w(\mathbf{x},t)|dt$.

The equivalent Von-Mises Strain (VMS), σ_v (Eq. (4)) was computed as well (being mainly used in material failure theory[29])

$$\sigma_v = \sqrt{\frac{3}{2} S_{ij} S_{ij}}, \tag{4}$$

where S_{ij} are the components of the stress deviator tensor $\sigma^{\mathrm{dev}} = \sigma - \frac{1}{3}(\mathrm{th}\sigma)I$.

2.3. *Boundary conditions*

The boundary conditions simulated the internal cardiovascular system of the brain and these ones should be adjusted to maximize the real conditions, being an important role in the development of the flow inside each artery. The pressure difference was another important factor that it was assumed to be only a function of time, and it was generated by a pulse wave of a finite velocity.[30]

Considering the fluid flow inside a circular artery, we used a derivation of a superposition of Womersley velocity profiles assuming that the flow is periodic in time to obtain the physiological flow conditions at the artery inlet.[31,32]

The velocity profile is shown in Eq. (5) (see more details of Womersley velocity profile in Ref. 20).

$$v(r,t) = \frac{2Q_0}{\pi a^2}\left[1 - \left(\frac{r}{a}\right)^2\right] + \sum_{n=1}^{N} \frac{Q_n}{\pi a^2}\left[\frac{1 - \frac{J_0\left(\frac{\beta_n r}{a}\right)}{J_0(\beta_n)}}{1 - \frac{2J_1(\beta_n)}{\beta_n J_0(\beta_n)}}\right] e^{in\omega t} \tag{5}$$

with $\beta_n = i^{\frac{3}{2}}\alpha_n = i^{\frac{3}{2}} a\sqrt{\frac{n\omega}{\nu}}$.

where α_n is the n-Womersley number (WN, we considered the equivalent radius of the entrance of the aneurysm as a predictor), a is the artery radius of the inlet, n is the number of modes, and ω is the angular frequency obtained from the period of the cardiac cycle. Equation (5) was used in each aneurysm as follows. First, an average of 60 velocity pulses of different patients was measured in their internal carotid artery using a Doppler ultrasound technique (shown in Fig. 4(a)). Second, the blood flow was calculated using the inlet-area of each case. Lastly, the blood flow was fitted using Fourier series, obtaining all coefficients Q_n. In our study, we have chosen eight modes and an angular frequency of $7.703\,\mathrm{s}^{-1}$ (period of the cardiac cycle was 0.857 s).[33]

In the outlet conditions, a normal pulsatile pressure was used between 80 mmHg and 120 mmHg[34] (represented in 4(b)), calculated through a three-element Windkessel model.[35]

According to the walls, the no-slip conditions were applied for each artery. On the other hand, in the mechanics boundary conditions, we used a fixed support in the inlet and outlets and an external constant pressure of 400 Pa simulating the outside environment of the arteries.[25]

All models and simulations were paralyzed and realized using double precision on a computer with 32 GB RAM and Intel i7 CPU with 8 cores.

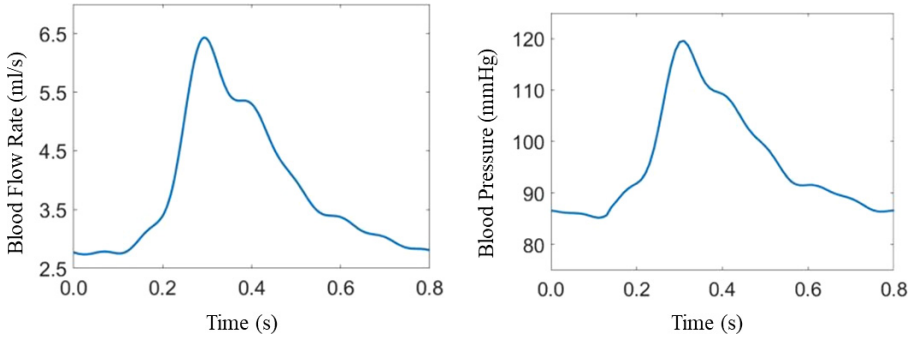

Fig. 4. (a) Blood flow rate used in the inlet condition. (b) Pulsatile pressure computed by the three-element Windkessel model.

2.4. *Statistic test and machine learning algorithms*

All parameters calculated from each geometry and the results of FSI simulations were analyzed such as features to predict the rupture risk of the aneurysms. We used five probability predictive models[36–38] to find the best: Bayesian Generalized Linear Model (BGLM), Logistic Regression (LR), Random Forest (RF), Adaptative Boosting (AdaBoost) and Probabilistic Neural Network (PNN), where we considered standardized parameters and the variation in the AUC-ROC. Also, we employed a 60% of the data for training set and 40% for the test set, where we used an exhaustive cross-validation with 10-folds. Also, an analysis of variance (ANOVA) and Kolmogorov–Smirnov (KS) test were applied to assess the statistical significance of abnormally distributed data, considering a P value below 0.05 and F-distribution above 4.[39]

3. Results and Discussion

3.1. *Simulation results*

RRT and VMS (Fig. 5(a)) were computed by Ansys software in all simulations. In each result of the simulations, we noted that the WSS was mainly located at the neck of the aneurysm due to the velocity vector (Fig. 5(b)) inside of the cerebral artery was approximately 90° (AIA) with respect to the wall of a saccular aneurysm[40] forming vorticities without being significant at the dome[41,42] (more results are shown in Fig. 6).

3.2. *Statistical analysis*

We analyzed the statistical significance of all parameters from FSI simulations and the morphological parameters through ANOVA and KS statistic tests, then,

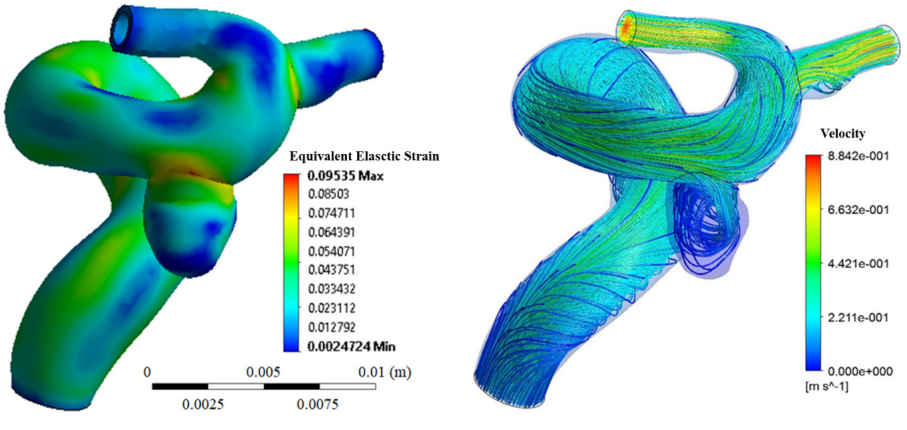

(a) (b)

Fig. 5. (a) Equivalent elastic strain (VMS) and (b) velocity streamline computed at a systolic time from ANSYS software.

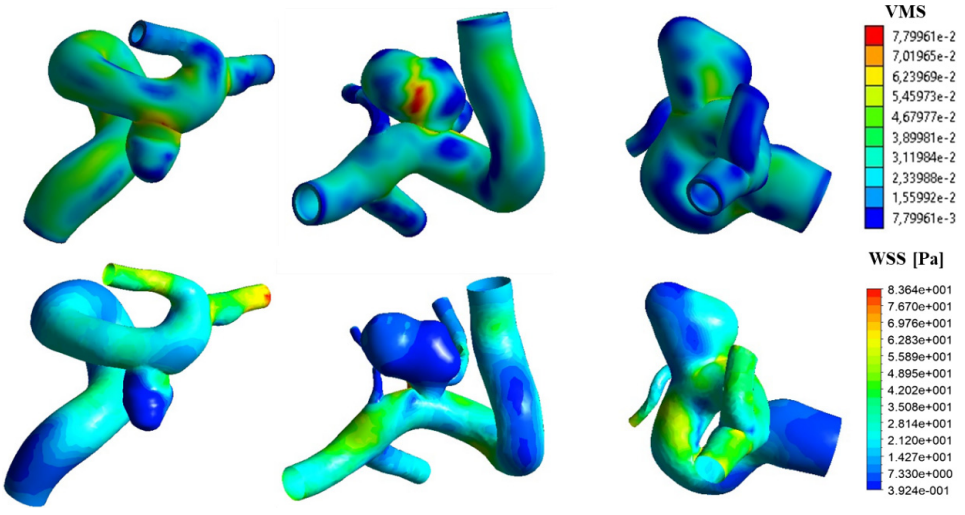

Fig. 6. Standardized results of VMS and WSS calculation at the systolic time in 3 random aneurysms selected.

Table 2. Statistic of the predictors used on the predicted models.

	Statistic	WN	RRT 10^{-3} (Pa^{-1})	VMS	MH (mm)	AR	BNF
Ruptured (30 cases)	Min.	0.196	399	0.00346	2.049	0.854	0.633
	1st Qu.	2.687	586	0.0452	5.178	1.294	1.187
	Median	3.303	886	0.0837	6.942	1.690	1.453
	Mean	3.004	963	0.0781	7.050	1.930	1.819
	3rd Qu.	3.362	1.10	0.104	8.188	2.303	2.157
	Max.	3.985	4.63	0.171	22.885	5.279	6.316
Unruptured (30 cases)	Min.	1.404	292	0.00225	1.510	0.634	0.574
	1st Qu.	2.423	355	0.0128	3.197	1.054	1.012
	Median	2.963	492	0.0223	5.153	1.341	1.176
	Mean	2.871	624	0.0227	5.655	1.388	1.372
	3rd Qu.	3.285	800	0.0301	7.117	1.551	1.645
	Max.	4.104	195	0.0493	21.321	3.860	2.854
All cases (60)	*F*-value	5.521	6.704	>10	>10	9.968	4.215
	P-value	0.00823	<0.001	<0.001	<0.001	0.00263	0.0095

we selected the predictors (shown in Table 2) in accordance with the P (smallest quantity of them) and F-distribution tolerance values.

It is observed in Table 2 that all quantities had higher value of the mean in the ruptured than in the unruptured group, in accordance with the results obtained by Xiang *et al.*[43] Whether the height of the aneurysm is higher in the ruptured group, the fluid has more distance to the maximum height, being less significant the TAWSS at the dome, and on average, in the aneurysm. In the same way, it occurred whether the neck of the aneurysm is lower in the ruptured group where less fluid enters to the aneurysm, resulting in a lower value of the TAWSS as well.

On the other hand, four morphological parameters were less statistically significant than AR and BNF: NSI, AIA, volume and area of the aneurysm, which is in good agreement with previous works.[44] In the same way, it happened with the TAWSS and OSI compared with RRT.[15,43,45] With respect to the mechanical parameters, we found that the best statistical significance was the VMS. Finally, the age and the gender of the patients were not statistically significant, following the results obtained by Lin *et al.*[46]

3.3. *Machine learning models*

We used five machine learning models to predict the rupture risk ("unruptured" was the positive class) of the cerebral aneurysm, where 36 samples were trained with six predictors from morphological parameters and FSI simulations. It is important to note that some authors indicated the existence of relevant parameters such as SR, TAWSS and OSI.[43] Also, other authors[47] concluded that the morphological parameters are the most relevant as predictors. However, this depends largely of the location of the aneurysms and the human conditions, thus, the literature available may provide the correct answer about the most relevant parameters depending on the reference conditions. In Fig. 7(a), the AUC fitted in the five models with all database is shown, where the AdaBoost model was the best, followed very closely by PNN, RF and BGLM. On the other hand, to validate each model, a cross-validation methodology was implemented with 10-folds, repeated 3 times. In Fig. 7(b), the ROC curves and the AUC were calculated in the test set of each model using 24 out-of-samples. Comparing the results of Figs. 7(a) and 7(b) we noted that the AUC position of the models was the same in both cases.

Xiang *et al.*,[43] Qin *et al.*,[47] Jing *et al.*[48] and Fan *et al.*[49] achieved to obtain an AUC over 70% using morphological, biological or hemodynamical predictors separately. When we combined these parameters we found that the best prediction

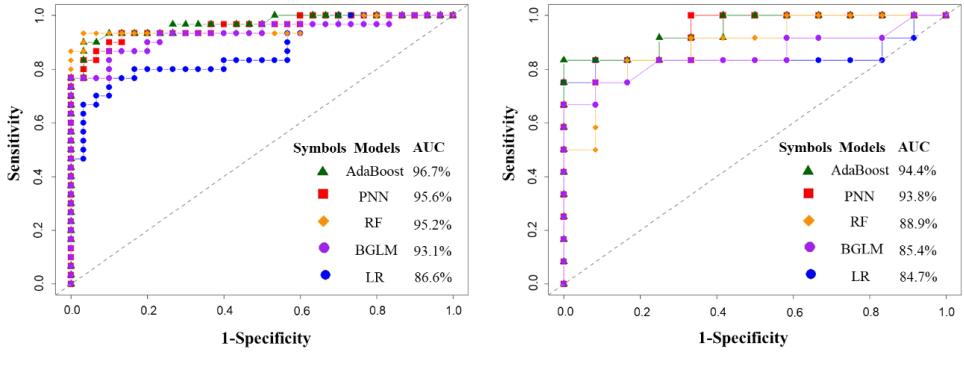

(a) (b)

Fig. 7. ROC curves for the (a) complete database and (b) predictive models used in the rupture risk of the aneurysms.

Table 3. Confusion matrix for the test set using AdaBoost algorithm.

Prediction	Unruptured	Ruptured
Unruptured	7	1
Ruptured	0	6

Table 4. Statistics parameters for the validation of the AdaBoost model.

Statistic parameter	Value
Accuracy	0.9286
P-value	<1e-4
95% CI	(0.8613, 0.9982)
Kappa	0.8971
Sensitivity	1.0000
Specificity	0.8571
Positive predictive value	0.8750
Negative predictive value	1.0000

model was AdaBoost with a 94.4% in the AUC (a confusion matrix and statistic parameters are shown in Tables 3 and 4, respectively. It is important to note that for small dataset the AUC-ROC shows more evidence in the model evaluation), where this is in accordance with the current results in the machine learning predictions and competitions about the best models to predict problems.[50,51] The PNN was very close to the first, with a 93.8% in AUC, however in the computing time AdaBoost was better. Likewise, we proved other combinations between predictors, e.g., AR, TAWWS, deformation, Re number, BNF and volume of the aneurysm and the value of AUC-ROC was less than the result shown in Fig. 7, in all the algorithms. In situations that involves the life or death of people, we need to have an accuracy as close as possible to 100%. This is possible according as we increase the number of predictors in the model, as indicated by Kohavi *et al.*,[52] or using reinforced learning algorithms, however in both cases it would imply having more patient data, being a very difficult task to fulfill. Although undoubtedly, the results obtained in this investigation may be used as support for neurosurgeons. In addition, when we select the best combination between morphological, mechanical, hemodynamical, biological and chemical parameters (being statistically significant) we could obtain better results. All these indicate that more studies are necessary to improve the results of machine learning algorithms.

4. Conclusions

Morphological, hemodynamical and mechanical parameters were analyzed with an ANOVA test, to determine the statistic significant used to predict the rupture risk of cerebral aneurysms. Using only computational tools, we reconstructed real

aneurysms by angiography images, then we simulated the intracranial blood flow using FSI on the Ansys software. We found that WM, RRT, VMS, MH, AR and BNF were the most significant parameters. Using all quantities, we computed five machine learning algorithm models, obtaining that the best AUC was the AdaBoost model using a cross-validation as a validation test in out-of-sample. On the other hand, morphological parameters are easy to calculate from a medical image, but the predictions are not good in accuracy, however we may improve the accuracy using FSI simulations and machine learning models, being relatively a fast task to carry out.

Acknowledgments

Alfredo Aranda-Núñez would like to thank CONICyT/PCHA PhD fellowship No. 21140180.

References

1. Brisman J, Song J, Newell D, Cerebral aneurysms, *New Engl J Med* **355**:928–939, 2006.
2. Keedy A, An overview of intracranial aneurysms, *McGill J Med* **9**(2):141–146, 2006.
3. M. Pritz, Cerebral aneurysm classification based on angioarchitecture, *J Stroke Cerebrovasc Dis* **20**(2):162–167, 2011.
4. Steiger H, Pathophysiology of development and rupture of cerebral aneurysms, *Acta Neurochir Suppl* **48**:1–57, 1990.
5. Phil W, Stehbens D, Etiology of intracranial berry aneurysms, *J Neurosurg* **70**(6):823–931, 1989.
6. Liang L, Liu M, Martin C, Elefteriades J, Sun W, A machine learning approach to investigate the relationship between shape features and numerically predicted risk of ascending aortic aneurysm, *Biomech Model Mechanobiol* **16**(5):1519–1533, 2017.
7. Mocco J, Brown R, Torner J, Capuano A, Fargen K, Raghavan M, Piepgras D, Meissner L, Huston J, Aneurysm morphology and prediction of rupture: An international study of unruptured intracranial aneurysms analysis, *Neurosurgery* **82**(4):491–496, 2018.
8. Canchi T, Kum D, EY N, Narayanan S, A review of computational methods to predict the risk of rupture of abdominal aortic aneurysms, *BioMed Res Int* **2015**(861627):12, 2015.
9. Cebral J, Mut F, Weir J, Putman C, Association of hemodynamic characteristics and cerebral aneurysm rupture, *Am J Neurorad* **32**:264–270, 2011.
10. Cebral J, Mut F, Weir J, Putman C, Quantitative characterization of the hemodynamic environment in ruptured and unruptured brain aneurysms, *Am J Neurorad* **32**:145–151, 2011.
11. Tan F, Torii R, Borghi A, Mohuaddin R, Wood N, Xu X, Fluid-structure interaction analysis of wall stress and flow patterns in a thoracicaortic aneurysm, *Int J Appl Mech* **1**(1):179–199, 2009.
12. Shum J, Elena S, Satish C, Finol E, Machine learning techniques for the assessment of AAA rupture risk, *ASME 2011 Summer Bioengineering Conf*, Pennsylvania, 2011.
13. Muluk S, Muluk P, Shium J, Finol E, On the use of geometric modeling to predict aortic aneurysm rupture, *Ann Vascul Surg* **44**:190–196, 2017.

14. Liu J, Chen Y, Lan L, Lin B, Chen W, Wang M, Li R, Yang Y, Zhao B, Duan Y, Prediction of rupture risk in anterior communicating artery aneurysms with a feed-forward artificial neural network, *Europ Radiol* **17**:1–8, 2018.
15. Valencia A, Morales H, Rivera R, Galvez M, Blood flow dynamics in patient-specifc cerebral aneurysm models: The relationship between wall shear stress and aneurysm area index through a stenosis, *Med Eng Phys* **30**(3):329–340, 2008.
16. Lv N, Tang H, Chen S, Wang X, Fang Y, Karmonik C, Huang Q, Liu J, Morphological parameters related to aneurysm wall enhancement in patients with multiple intracranial aneurysms, *World Neurosurg* **18**:338–343, 2018.
17. Hunter J, A method of raising the specific gravity of the blood, *J Physiol* **11**(1–2):115–120, 1890.
18. Hipple J, *Chemical Engineering for Non-Chemical Engineers*, ALChE, New Jersey, 2017.
19. Brust M, Schaefer C, Doerr R, Pan L, Garcia M, Arratia P, Wagner C, Rheology of human blood plasma: Viscoelastic versus newtonian behavior, *Phys Rev Lett* **110**(7):078305, 2013.
20. Zamir M, *The Physics of Pulsatile Flow*, Springer, New York, 2000.
21. Cipolla M, *The Cerebral Circulation*, Morgan & Claypool Life Sciences, San Rafael, 2009.
22. Humphrey J, Canham P, Structure, mechanical properties, and mechanics of intracranial saccular aneurysms, *J Elast* **61**:49–81, 2000.
23. Olugsen M, Peskin C, Kim W, Pedersen E, Nadim A, Larsen J, Numerical simulation and experimental validation of blood flow in arteries with structured-tree outflow conditions, *Ann Biomed Eng* **28**(11):1281–1299, 2000.
24. Valencia A, Contente A, Ignat M, Mechanical test of human cerebral aneurysm specimens obtained from surgical clipping, *J Mech Med Biol* **15**(5):1–12, 2015.
25. Valencia A, Burdiles P, Ignat M, Mura J, Bravo E, Rivera R, Sordo J, Fluid structural analysis of human cerebral aneurysm using their own wall mechanical properties, *Comput Math Methods Med* **18**, 2013.
26. Benra F, Dohmen H, Pei J, Schuster S, Wan B, A comparison of one-way and two-way coupling methods for numerical analysis of fluid-structure interactions, *J Appl Math* **2011**:853560, 2011.
27. Himburg H, Gizybowski A, Hazel D, LaMack A, Li X, Friedman M, Spatial comparison between wall shear stress measures and porcine arterial endothelial permeability, *Am J Physiol* **5**:16–22, 2004.
28. Lee S, Antiga L, Steinman D, Correlations among indicators of disturbed fow at the normal carotid bifurcation, *J Biomech Eng* **131**(6):031013, 2009.
29. Christensen R, *The Theory of Materials Failure*, Oxford University Press, Rhode Island, 2013.
30. Womersley J, Method for the calculation of velocity, rate of flow and viscous drag in arteries when the pressure difference is known, *J Physiol* **127**(3):553–563, 1955.
31. Cebral J, Castro M, Soto O, Lohner R, Alperin N, Blood-flow models of the circle of Willis from magnetic resonance, *J Eng Math* **47**(3–4):369–386, 2003.
32. Cebral J, Castro M, Appanaboyina S, Putman C, Millan D, Frangi A, Efficient pipeline for image-based patient-specific analysis of cerebral aneurysm hemodynamics: Technique and sensitivity, *IEEE Trans. Med. Imag.* **24**(4):457–467, 2005.
33. Nengom J, Sap S, D. Chelo, Mbono R, Boombhi J, Mouafo F, Chiabi A, Kingue S, Assessment of cardiac function in children with congenital adrenal hyperplasia: A case control study in Cameroon, *BMC Pediat* **17**(109):1–8, 2017.

34. Ogedegbe G, Pickering T, Dphil M, Principles and techniques of blood pressure measurement, *Cardiol Clin* **28**(4):571–586, 2010.
35. Westerhof N, Bosman F, De Vries CJ, Noordergraaf A, Analog studies of the human systemic arterial tre, *J Biomech* **2**(2):121–134, 1969.
36. Dunning T, Friedman E, *Machine Learning Logistics: Model Management in the Real World*, O'Reilly, California, 2017.
37. Witten I, Frank E, Hall M, Pal C, *Data Mining: Practical Machine Learning Tools and Techniques*, Morgan Kaufmann — Elsevier, Cambridge, 2017.
38. Freund Y, Schapire R, A short introduction to boosting, *J Japan Soc Artif Intell* **14**(5):771–780, 1999.
39. Cardinal R, Aitken M, *ANOVA for the Behavioral Sciences Researcher*, Psychology Press, 2005.
40. Lee T, Borazjani I, Sotiropoulos F, Pulsatile flow effects on the hemodynamics of intracranial aneurysm, *J Biomech Eng* **132**(11):1–11, 2010.
41. Rossmann C, Fisher J, Effect of non-newtonian behavior on hemodynamics of cerebral aneurysms, *J Biomech Eng* **131**(9), 2009.
42. Pereira V, Brina O, Gonzalez A, Narata A, Bijilenga P, Schaller K, Lovlad K, Ouared R, Evaluation of the influence of inlet boundary conditions on computational fluid dynamics for intracranial aneurysms: A virtual experiment, *J Biomech* **46**(9):1531–1539, 2013.
43. Xiang J, Natarajan S, Tremmel M, Ma D, Hopkins L, Siddiqui A, Levy E, Meng H, Hemodynamic-morphologic discriminants for intracranial aneurysm rupture, *Stroke* **42**(1):144–152, 2011.
44. Dhar S, Tremmel M, Mocco J, Minsouk M, Yamamoto J, Siddiqui A, Hoplins L, Meng H, Morphology parameters for intracranial aneurysm rupture risk assessment, *Neurosurgery* **63**(2):185–197, 2008.
45. Xu J, Yu Y, Wu X, Wu Y, Jiang C, Wang S, Huang Q, Liu J, Morphological and hemodynamic analysis of mirror posterior communicating artery aneurysms, *PlosOne* **8**(1):1–7, 2013.
46. Lin N, Ho A, Charoenvimolphan N, Frerichs K, Day A, Du R, Analysis of morphological parameters to differentiate rupture status in anterior communicating artery aneurysms, *PlosOne* **8**(11), 2013.
47. Qin H, Yang Q, Zhuang Q, Long J, Yang F, Zhang H, Morphological and hemodynamic parameters for middle cerebral artery bifurcation aneurysm rupture risk assessment, *J Korean Neurosurg Soc* **60**(5):504–510, 2017.
48. Jing L, Fang J, Wang Y, Li H, Wang S, Yang X, Zhang Y, Morphologic and hemodynamic analysis in the patients with multiple intracranial aneurysms: Ruptured versus unruptured, *PlosOne* **10**(7), 2015.
49. Fang J, Wang Y, Liu J, Zhang Y, Morphological-hemodynamic characteristics of intracranial bifurcation mirror aneurysms, *World Neurosurg* **84**(1), 2015.
50. Olivera A, Roesler V, Iochpe C, Schmidt M, Barreto S, Duncan D, Comparison of machine-learning algorithms to build a predictive model for detecting undiagnosed diabetes — ELSA-Brasil: Accuracy study, *Sao Paulo Med J* **135**(3):234–246, 2017.
51. Friedman J, Greedy function approximation: A gradient boosting machine, *Ann Statist* **29**(5):1189–1232, 2001.
52. Kohavi R, A study of cross-validation and bootstrap for accuracy estimation and model selection, *Proc. 14th Int Joint Conf Artifical Intelligence*, Vol. 2, pp. 1137–1145, 1995.